International Journal of Automotive Technology, Vol. 19, No. 1, pp. 135–146 (2018)
DOI 10.1007/s12239–018–0013–4

pISSN 1229–9138/ eISSN 1976–3832

DYNAMICS CHARACTERISTICS ANALYSIS AND CONTROL OF FWID EV

Dongmei Wu[1, 2, 3], Haitao Ding[1)*] and Changqing Du[2, 3]

[1)]State Key Laboratory of Automotive Simulation and Control, Jilin University, Changchun 130033, China
[2)]Hubei Key Laboratory of Advanced Technology of Automotive Components, Wuhan University of Technology, Wuhan 430070, China
[3)]Hubei Collaborative Innovation Center for Automotive Components Technology, Wuhan University of Technology, Wuhan 430070, China

(Received 18 April 2016; Revised 14 May 2017; Accepted 13 August 2017)

ABSTRACT–Compared with internal combustion engine (ICE) vehicles, four-wheel-independently-drive electric vehicles (FWID EV) have significant advantages, such as more controlled degree of freedom (DOF), higher energy efficiency and faster torque response of an electric motor. The influence of these advantages and other characteristics on vehicle dynamics control need to be evaluated in detail. This paper firstly analyzed the dynamics characteristics of FWID EV, including the feasible region of vehicle global force, the improvement of powertrain energy efficiency and the time-delays of electric motor torque in the direct yaw moment feedback control system. In this way, the influence of electric motor output power limit, road friction coefficient and the wheel torque response on the stability control, as well as the impact of motor idle loss on the torque distribution method were illustrated clearly. Then a vehicle dynamics control method based on the vehicle stability state was proposed. In normal driving condition, the powertrain energy efficiency can be improved by torque distribution between front and rear wheels. In extreme driving condition, the electric motors combined with the electro-hydraulic braking system were employed as actuators for direct yaw moment control. Simulation results show that dynamics control which take full advantages of the more controlled freedom and the motor torque response characteristics improve the vehicle stability better than the control based on the hydraulic braking system of conventional vehicle. Furthermore, some road tests in a real vehicle were conducted to evaluate the performance of proposed control method.

KEY WORDS : Four-wheel-independently-drive electric vehicles (FWID EV), Dynamics characteristics, Powertrain energy efficiency, Vehicle stability, Dynamics control

1. INTRODUCTION

As the issues of global energy crisis and environmental pollution have become increasingly prominent, the sustainable development of automotive industry is necessary. Electric vehicles (EV) are considered as one of the effective solutions (Lv *et al*., 2015). On the other hand, with the development of electric driving system and electric control system, some advanced EV structures have been researched, such as EV with driveline system which can distribute the driving torque between axles or between right and left wheels of the same axle (Kim *et al*., 2015), and four-wheel-independently-drive (FWID) EV with four in-wheel electric motors (Ivanov *et al*., 2015). Among these new vehicle structures, FWID EV increase the controllable DOF significantly. Besides, compared with internal combustion engine (ICE), electric motor driving system, especially the in-wheel motor, has higher energy efficiency and better torque response performance. As a result, FWID EV have received much attention in recent years.

Hori (2004) indicated the advantages of EV in the electric motor torque control which will be of benefit to vehicle dynamics control. However, the characteristics and advantages of FWID EV should be evaluated in detail, which will provide guidance for dynamics control. The independent control of each wheel torque supplies more DOF of torque distribution. For conventional ICE vehicle, Keiji (1989, 1990), Sawase and Ushiroda (2008) and Klomp (2011) investigated the impact of torque distribution mode between front and rear wheels, as well as that between left and right wheels, on the vehicle dynamics performance, including the driving and braking performance in longitudinal direction, and the limit performance in lateral direction. For several different vehicle configurations: two wheel dependently driven by ICE, two rear wheels independently driven by electric motor and FWID vehicle, Jonasson *et al*. (2010) used the brute-force method to compare the attainable vehicle global force. And then it was proved that FWID vehicle can reach much better

**Corresponding author*. e-mail: dinght@jlu.edu.cn

performance than the conventional two-wheel-drive vehicle in dynamics control system (Jonasson *et al*., 2011). Some of the analysis methods in above literatures can be used to analyze the dynamics characteristics of FWID EV. However the influence of electric motor output power limit, road friction coefficient and the wheel torque response need to be further considered for FWID EV.

In addition to the dynamics characteristics, the energy efficiency of the FWID EV power system is quite different from the ICE vehicles. For FWID EV, the powertrain consists of four electric motors, which can be considered as four power sources. The energy efficiency of electric motor varies with the operating point, i.e., the torque and rotation speed. Therefore, in literatures (Chen and Wang, 2011, 2014; Park *et al*., 2015; Dizqah *et al*., 2016), the torque distribution of FWID EV was investigated to achieve the maximum energy efficiency of drivetrain. However, the optimal allocation solution given in different literatures were not exactly identical and the impact of motor idle loss was not explicitly stated.

Actually, the driving system of FWID EV is an over-actuated system and the control allocation method can be used in dynamics control (Johansen and Fossen, 2013; Yu *et al*., 2014). Shuai *et al*. (2014) and Xiong *et al*. (2016) adopted the quadratic programming (QP) based torque allocation algorithm with the advantage of equally and reasonably utilizing the tire-road friction. Novellis *et al*. (2014) compared four different control allocation objective functions, which are based on the drivetrain input power, the longitudinal tire slip, the longitudinal slip power loss and the combined tire force coefficient, respectively. And more importantly, multi-objectives about the driving safety and energy saving can be uniformly applied in dynamics control of FWID EV (Lin and Xu, 2015). Despite a variety of control methods, an important part of the FWID EV dynamics control system is still the direct yaw moment control (DYC), which is considered an effective method to improve the vehicle stability and steering characteristics (Yim, 2017; Yin and Hu, 2014). For DYC system, hierarchical control is a commonly used architecture. In the upper layers, the required direct yaw moment can be determined by many different control methods, such as robust control (Yin *et al*., 2015; Hu *et al*., 2017), model predictive control (Zhao *et al*., 2015) and so on. In the lower layers, the electric motors can be combined with the mechanical braking system to generate yaw moment for stability control through different cooperative methods (Emırler *et al*., 2015; Ko *et al*., 2016).

The above control methods improves the dynamics performance of FWID EV significantly. However, it is still difficult to distinguish the advantages of control method and that of vehicle configuration. The aim of this paper is to evaluate the characteristics of FWID EV, especially the influence of electric motor output power limit, road friction coefficient and the wheel torque respond on the stability control, as well as the impact of motor idle loss on the torque distribution method. Firstly, the analysis was conducted through theoretical methods. Then a basic but practical control strategy was developed to take full advantages of the dynamics characteristics. By comparing with the same control method of conventional vehicle, the characteristics and advantages of FWID will be evaluated and validated explicitly.

This paper was organized as follows: firstly, the feasible region of vehicle global force was analyzed in Section 2; then the improvement of powertrain energy efficiency was conducted in Section 3; also the time-delay of electric motor and hydraulic braking system in the direct yaw moment feedback control system were compared in Section 4; based on the analysis results, the FWID EV dynamics control strategy taking full advantages of the dynamics characteristics was studied to improve vehicle stability safety and powertrain energy efficiency in Section 5; In Section 6, some simulation and road tests results were analyzed.

2. FEASIBLE REGION OF VEHICLE GLOBAL FORCE

For the existing vehicle equipped with electronic stability control system, the braking pressure and braking torque of four wheels can be controlled independently in case of emergency. For FWID EV, both the braking torque and driving torque of four wheels can be controlled independently and the number of dynamics controlled DOF increases significantly. This provides the possibility to enlarge the available vehicle global force region, which will improve the vehicle dynamics controlled range.

2.1. Feasible Region without Electric Motor Power Limit

For the existing vehicle equipped with electronic stability control system, the braking pressure can be controlled independently. The constraints of tire force can be expressed as follows (Jonasson *et al*., 2010):

$$\begin{cases} \left(\dfrac{F_{yi}}{F_{y0}}\right)^2 + \left(\dfrac{F_{xi}}{F_{imax}}\right)^2 \le 1 \\ -F_{imax} \le F_{xi} \le 0 \end{cases} \tag{1}$$

where F_{xi} and F_{yi} are the longitudinal and lateral tire force of each wheel (i = 1, 2, 3, 4), F_{y0} is the initial lateral tire force, *i.e.* the lateral force generated by steering wheel angle when there is no differential driving/braking, F_{imax} is the maximum tire force, which can be calculated through the tire-road friction coefficient and the wheel vertical load, simply by $F_{imax} = \mu F_{zi}$. The first inequality constraint means that the tire longitudinal force and lateral force are limited by the friction ellipse. The second inequality constraint means that only the braking torque can be controlled actively. Here it is assumed that the hydraulic braking pressure is sufficient, and the tire braking force is only limited by the maximum tire force.

For FWID EV, both the braking pressure and the driving torque can be controlled independently. The tire force limitation can be expressed as follows:

$$\begin{cases} \left(\frac{F_{yi}}{F_{y0}}\right)^2 + \left(\frac{F_{xi}}{F_{max}}\right)^2 \le 1 \\ -F_{imax} \le F_{xi} \le F_{imax} \end{cases} \quad (2)$$

Here the limitation of the electric motor torque output is neglected temporarily and the tire driving force is just limited by the maximum tire force as in Equation (1).

Then the vehicle global longitudinal force, lateral force and yaw moment can be expressed by tire forces:

$$\begin{bmatrix} F_x \\ F_y \\ M_z \end{bmatrix} = A \cdot \left[F_{x1}, F_{x2}, F_{x3}, F_{x4}, F_{y1}, F_{y2}, F_{y3}, F_{y4} \right]^T \quad (3)$$

where A is the transfer matrix decided by steering wheel angle δ, the distance between center of gravity (C.G.) and the front axle L_a, the distance between C.G. and the rear axle L_b and the tread L_c.

In order to analyze the available maximum global force, here we just consider the maximum tire force. So the first inequality constrains in Equations (1) and (2) can be converted to equality. After discretization, all possible longitudinal tire force satisfying the second inequality constraint are chosen to calculate the available maximum lateral force according to the first equality constrain. Then the corresponding available maximum vehicle global force and moment in different longitudinal tire force can be obtained. In this way, the available vehicle lateral force and yaw moment range in different vehicle configuration can be compared.

A steady steering condition is chosen to determine the initial state, where the tire-road friction coefficient is set as 0.8, the steering wheel angle is 60 deg, and the vehicle speed is 80 km/h. With the maximum tire force and initial lateral force of each wheel in steady-state condition, the available vehicle lateral force and yaw moment in different longitudinal tire force are shown in Figure 1. In the figure, the red area represents the four wheels independently brake vehicle limited by Equation (1). The black area represents the enlarged areas of FWID vehicle compared with the four wheel independently brake vehicle. It can be seen that the FWID configuration enlarges the available vehicle lateral force and vehicle yaw moment significantly. It indicates the potential in improving the vehicle dynamics controllability.

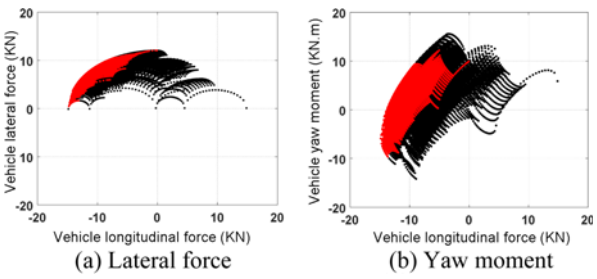

(a) Lateral force (b) Yaw moment

Figure 1. Available global force without electric motor power limit when tire-road friction coefficient is 0.8: Four wheel independently brake vehicle (red) and the enlarged area of FWID vehicle (black) (For interpretation of the references to color in this figure legend, the reader is referred to the web version of this article.).

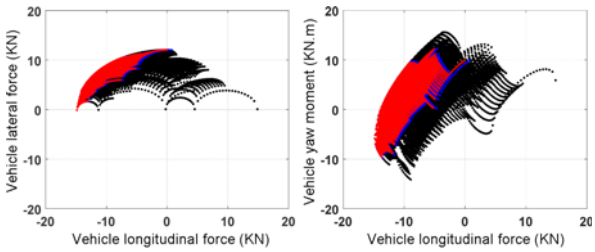

(a) Lateral force (b) Yaw moment

Figure 2. Available global force with electric motor power limit when tire-road friction coefficient is 0.8: Four wheel independently brake vehicle (red), the enlarged area of FWID vehicle without driving torque limit (black) and the enlarged area of FWID EV with driving torque limit (blue) (For interpretation of the references to color in this figure legend, the reader is referred to the web version of this article.).

2.2. Feasible Region with Electric Motor Power Limit

The maximum output power of electric motor, especially in-wheel electric motor, is generally smaller than ICE and hydraulic braking system. So the effect of the electric motor power limit must be considered. Here the maximum torque output of each electric motor is limited to 150 Nm, and the test condition is the same as in Section 2.1 when the tire-road friction coefficient is set as 0.8. The enlarged region of available vehicle lateral force and yaw moment are shown in Figures 2 (a) and (b) in blue color,

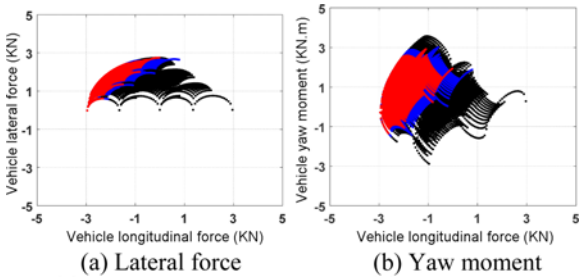

(a) Lateral force (b) Yaw moment

Figure 3. Available global force with electric motor power limit when tire-road friction coefficient is 0.2: Four wheel independently brake vehicle (red), the enlarged area of FWID vehicle without driving torque limit (black) and the enlarged area of FWID EV with driving torque limit (blue) (For interpretation of the references to color in this figure legend, the reader is referred to the web version of this article.).

respectively. The results show that the FWID EV with driving torque limitation enlarge the controllable region little in high adhesion road.

Then a test in low adhesion road is conducted. The tire-road friction coefficient is set as 0.2, the steering wheel angle is 15 deg, and the vehicle speed is 80 km/h. With the same driving torque limitation, the results are shown in Figure 3. It can be seen that, when the tire adhesion ability is poor, the FWID EV can enlarge the controlled region of global force significantly even though with the driving torque limit.

3. IMPROVEMENT OF POWERTRAIN ENERGY EFFICIENCY

For FWID EV, the powertrain consists of four electric motors, which can be considered as four power sources. The tested energy efficiency of a permanent magnet synchronous (PMSM) in-wheel electric motor and the converter is given in Figure 4. It can be seen that the energy efficiency varies widely in different operation point.

From the perspective of driving system energy efficiency, the driving torque can be distributed through global optimization with the constraints of yaw moment and total driving torque. To simplify the optimization problem and minimize the impact on vehicle movement in lateral and yaw direction, this paper just distributes the driving torque between axles in normal driving condition. Then the axle torque is even distributed between left and right wheel when there is no direct yaw moment in normal stable driving condition.

With a certain power output, the driving system energy efficiency is equivalent with the power input. For distribution between axles, the objective function can be simplified to the following equation:

$$\min\ J_{\mathrm{p}} = \frac{W_{\mathrm{f}} T_{\mathrm{d}} \omega_{\mathrm{f}}}{\eta_{\mathrm{f}}} + \frac{(1 - W_{\mathrm{f}}) T_{\mathrm{d}} \omega_{\mathrm{r}}}{\eta_{\mathrm{r}}} \tag{4}$$

where W_{f} is the factor of front axle torque divided by the total torque, ω_{f} and ω_{r} are the average rotation speed of front axle and right axle respectively, η_{f} and η_{r} are the driving system efficiency of front axle and right axle respectively, which includes the efficiency of eclectic motor and the converter. The efficiency map can be obtained by experiment as shown in Figure 4.

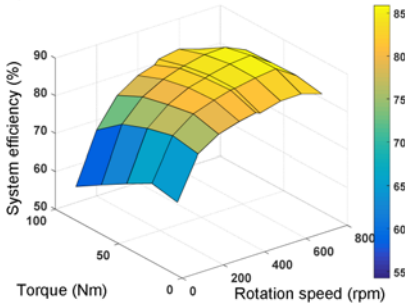

Figure 4. Efficiency map of an in-wheel electric motor.

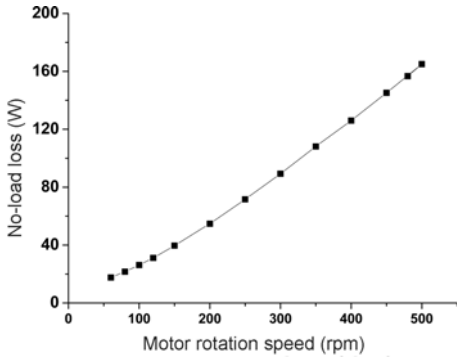

Figure 5. Idle power loss of the PMSM.

However, Equation (4) is applicable only when torque output of every electric motor is not zero. If there is electric motor with no torque output, the idle loss must be included. Then the optimization objective must be modified to the following equation:

$$\min J_{\mathrm{p}} = \begin{cases} \dfrac{W_{\mathrm{f}} T_{\mathrm{d}} \omega_{\mathrm{f}}}{\eta_{\mathrm{f}}} + \dfrac{(1 - W_{\mathrm{f}}) T_{\mathrm{d}} \omega_{\mathrm{r}}}{\eta_{\mathrm{r}}} & 0 < W_{\mathrm{f}} < 1 \\ P_{\mathrm{loss\_motor0}}(n_{\mathrm{f}}) + \dfrac{T n_{\mathrm{r}}}{\eta_{\mathrm{r}}} & W_{\mathrm{f}} = 0 \\ \dfrac{T n_{\mathrm{f}}}{\eta_{\mathrm{f}}} + P_{\mathrm{loss\_motor0}}(n_{\mathrm{r}}) & W_{\mathrm{f}} = 1 \end{cases} \tag{5}$$

where $P_{\mathrm{loss\_motor0}}(n)$ is the idle loss, which can be measured on the test bench at different rotation speeds in the idle operation condition. The idle friction torque of the PMSM is shown in Figure 5.

For the electric vehicle used in this paper, the static load of front axle is approximately equal to that of rear axle. As we know, the normal load on rear wheels increases and the normal load on front wheels load decreases, which will become opposite during deceleration. In order to make full use of the road adhesion condition and improve the vehicle driving and braking performance, the driving torque distributed to the rear wheels should be larger than the front wheels during acceleration, *i.e.*, the W_{f} smaller than 0.5. In contrast, the braking torque distributed to the front wheels should be larger than rear wheels during deceleration, *i.e.*, the W_{f} larger than 0.5. Therefore, the value of W_{f} has an upper limit of 0.5 in driving condition. Combined with total driving torque requirement and the torque output limitation of each axle, the constraints can be expressed as follows:

$$s.t \quad \begin{cases} 0 \le W_{\mathrm{f}} \le 0.5 \\ 0 \le T_{\mathrm{d}} W_{\mathrm{f}} \le T_{\mathrm{f\,max}} \\ 0 \le T_{\mathrm{d}} (1 - W_{\mathrm{f}}) \le T_{\mathrm{r\,max}} \end{cases} \tag{6}$$

where $T_{\mathrm{f\,max}}$ and $T_{\mathrm{r\,max}}$ are respectively the maximum torque of front axle and rear axle at current rotation speed.

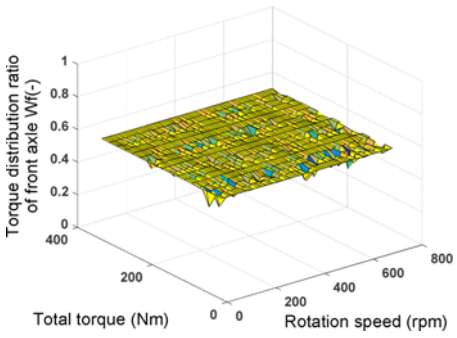

Figure 6. Optimal distribution coefficient of front axle obtained from offline optimization after considering the idle loss.

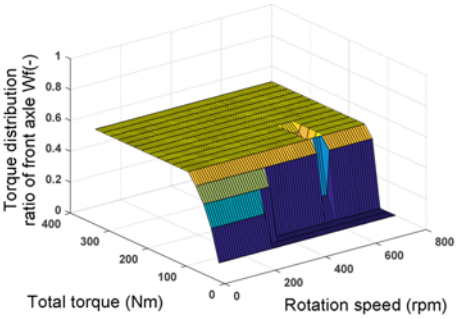

Figure 7. Optimal distribution coefficient of front axle obtained from offline optimization without considering the idle loss.

To reduce calculation load, a local optimization is conducted firstly. And then the local optimization results are compared manually to find the global optimization result. Based on the efficiency map of the electric motor powertrain system, the optimal distribution coefficient W_f can be obtained through offline optimization. Then the results can be expressed by another map related with the total driving torque requirement and electric motor rotation speed as shown in Figure 6, which can be used as lookup table in real control system. For comparison, the optimization results without considering the idle loss is given in Figure 7.

In Figure 7, because the idle loss is neglected, the optimal torque distribution ratio is about 0 when the total torque is quite small and then increases from 0 to 0.5 as the total torque increases. In Figure 6, after considering the no-load loss, the optimal distribution ratio is always around 0.5 with any total torque demand. It means that the driving torque should be equally distributed between axles for high driving system efficiency in most condition. Therefore, for the PMSM researched in this paper, the impact of idle loss on the torque distribution is significant. After considering the idle loss, the optimization objective function can reflect the system's real loss characteristic more accurately and the optimization results are more accurate.

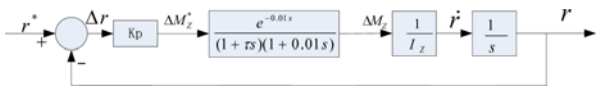

Figure 8. Direct yaw moment control system diagram when steering wheel input is zero.

4. TIME-DELAY OF DIRECT YAW MOMENT CONTROL SYSTEM

Compared with ICE and hydraulic braking system, the torque response of electric motor is much faster. Experiment results show that the response time of in-wheel electric motor torque control is less than 20 ms (Yu and Gong, 2008; Lu *et al*., 2009), while the electro-hydraulic braking system pressure control is about 50-60 ms (Wu *et al*., 2014; Lv *et al*., 2014, 2017). For ICE and conventional hydraulic braking system, the response time will be longer. So the torque response speed of electric motor is more than twice of the electro-hydraulic braking system.

In direct yaw moment control system, it can be assumed that the yaw moment consists of two parts. The first part is generated by the tyre lateral force caused by the steering wheel input, which can be seen as a feedforward input by driver. The second part is the direct yaw moment generated by the differential tyre longitudinal force, which is actuated by electric motor and hydraulic braking system. As is known to all, the response characteristic of actuator affects the time-delay of control system, which is important for the system relatively stability. Here the steering wheel input can be set to zero and just the direct yaw moment feedback control system is analyzed to evaluate the effect of the wheel torque response. For simplification, the desired yaw moment is decided by a proportional feedback control method. The diagram of direct yaw moment control system can be expressed as Figure 8.

In Figure 8, the input r^* is the reference yaw rate, which can be obtained from a reference vehicle model. Here it is just used as a followed target. Kp is the proportional factor of feedback control. ΔM_z^* is the required yaw moment. $e^{0.01s}$ represents communication delay, and $\frac{1}{1+\tau s}$ represents the response characteristic of wheel torque control, $\frac{1}{1+0.01s}$ represents the delay of the tire force generation, which is calculated when vehicle speed is 80 km/h and the tire relaxation length is 0.04 m. ΔM_Z is the generated yaw moment actually, and I_Z is the vehicle rotation inertia in yaw direction.

Let $\frac{Kp}{Iz} = P$, then the open-loop transfer function of the above system can be expressed as follows:

$$G(s) = P\frac{e^{-0.01s}}{s(1+\tau s)(1+0.01s)} \tag{7}$$

Then the close-loop transfer function can be expressed as follows:

$$H(s) = \frac{G(s)}{1 + G(s)} \tag{8}$$

According to the characteristic of first order system, the phase changes significantly with frequency and the amplitude changes little before the turning point frequency. Generally, the time constant τ of electric motor torque is smaller than 0.1 and the corresponding turning point frequency is 10 rad/s. While for most vehicles, the yaw rate response frequency will not exceed 1.5 Hz, *i.e.*, 9.42 rad/s. As a result, it can be considered that the time constant of electric motor torque control mainly affect the system phase.

The phase of open-loop control system can be expressed as follows:

$$\angle G(j\omega) = -0.01\omega - 90\text{deg} - \arctan\tau\omega - \arctan 0.01\omega \tag{9}$$

According to the frequency response range of vehicle yaw rate, the cut-off frequency of the system can be set as 10 rad/s. Strictly speaking, the open-loop phase margin is calculated at the frequency where the amplitude is 1. Here the analysis focuses on the system performance before the cut-off frequency, so the cut-off frequency is used to calculate the open-loop phase margin as follows:

$$\phi_{\text{pm}} = -0.01\omega_{\text{cc}} - 90\,\text{deg} - \arctan\tau\omega_{\text{cc}} - \arctan 0.01\omega_{\text{cc}} + 180\,\text{deg} \tag{10}$$

According to the test results, the time constant of electric motor torque control is about 0.01, and the open-loop phase margin is about 73 deg. While for hydraulic braking system, the time constant is larger than 0.02 and the open-loop phase margin is about 67 deg. As is known, open-loop phase margin is an important indicator for evaluating the system relative stability. A bigger value in appropriate range has advantage in improving the system performance (Ogata, 2009). Therefore, the electric motor should be fully utilized to improve the dynamic performance of direct yaw moment control.

5. DYNAMICS CONROL OF FWID EV

According to the above analysis of FWID EV characteristics, some conclusions can be obtained for dynamics control: to take full advantages of the controllable DOF, the control allocation of wheel torque can be used to improve the vehicle dynamics performance and driving system efficiency; because of the fast response and the power limitation, electric motor can be combined with hydraulic braking system to work as actuators of vehicle dynamics control system. To fully exploit its potential and advantages, dynamics control system taking full advantages of the characteristics can be deployed to improve the vehicle performance in vehicle safety and energy saving.

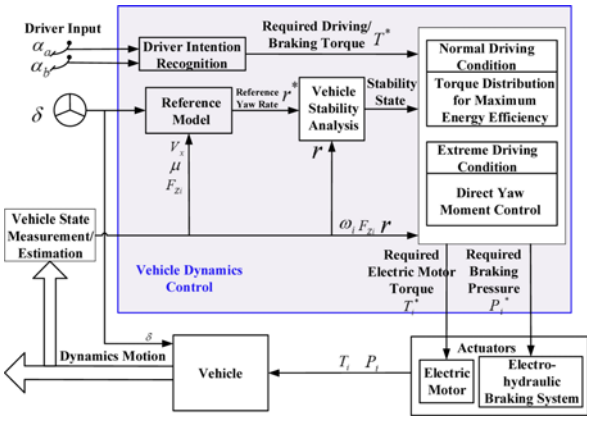

Figure 9. Structure of FWID EV dynamics control system.

5.1. Control System Structure

Based on the above control principle, the control system can be designed as shown in Figure 9. There are two control objectives for electric vehicle dynamics control: the vehicle dynamics safety and high powertrain energy efficiency. Sometimes the two control requirements are not consistent. For coordination, the driving condition is classified based on the vehicle stability analysis. When the stability is satisfactory, it is considered as normal driving condition. Then the high driving system efficiency can be the control objective, and the driving torque is optimally distributed between wheels for high driving efficiency. When the stability is poor, it is considered as extreme driving condition, and the vehicle stability safety must first be guaranteed. To take full advantages of the controllable DOF and the torque responsibility, the electric motor is applied to the stability control as actuators in addition to the conventional hydraulic braking system. Therefore, the additional yaw moment is generated by electric motor driving system and hydraulic braking system. The distribution of yaw moment between electric motors and the coordination of electric motor and hydraulic braking are necessary.

The FWID EV dynamics control system shown in Figure 9 includes several main blocks: measurement and estimation of vehicle state, vehicle stability analysis, driving torque optimal distribution for energy saving in normal driving condition and the stability control in extreme driving condition. Then the key blocks researched in this paper are the vehicle stability analysis, the driving torque optimal distribution for energy saving in normal driving condition and the stability control in extreme driving condition. Among the three blocks, the driving force optimal distribution for energy saving in normal driving condition just adopts the optimization results of Figure 6 in Section 3, which will not be repeated. Therefore, the other two blocks: the vehicle stability analysis and the stability control in extreme driving condition will be introduced in detail in the following sections.

5.2. Vehicle Stability Determination

Yaw rate is an important state reflecting the vehicle stability. It is generally believed that yaw rate reflects the steering intensity. In the stable state, the vehicle yaw rate r should follow a reference value r^* obtained from the reference vehicle model. The deviation should be kept within a certain range. If the deviation exceeds the limit, it is believed that there is a risk of unstable. Besides, sideslip angle also reflects the vehicle stability. However, at present, the measurement of sideslip angle is high cost and usually it needs to be estimated. Because of sensor deviation, noise, and dynamics model mismatch, it is difficult to estimate the sideslip angle accurately under various conditions either by kinematics-based methods or by vehicle-model-based method (Phanomchoeng *et al*., 2011; Piyabongkarn *et al*., 2009; Hac and Simpson, 2000). To estimate the sideslip angle more accurately, more sensors including the GPS and the camera are adopted (Yoon and Peng, 2014; Wang *et al*., 2014). Those sensors are expensive for mass produced conventional vehicle. Compared with sideslip angle, yaw rate can be measured easily in real vehicle. Therefore, the vehicle stability control based on yaw rate is often adopted (Hu *et al*., 2017; Kim *et al*., 2012).

If the Equation (11) is satisfied, the vehicle is considered as stable in normal driving condition. Otherwise, the vehicle is considered as unstable in the extreme driving condition.

$$\left|r - r^*\right| \le \Delta r_{\text{th}} \tag{11}$$

where Δr_{th} is a threshold determined by the steering wheel angle rate.

5.3. Direct Yaw Moment Control in Extreme Driving Condition

According to the vehicle stability analysis, while in extreme driving condition, direct yaw moment control is started. Compared with conventional ICE vehicle, the direct yaw moment control for FWID EV can take advantage of more controllable DOF and more actuators. The structure diagram of direct yaw moment control is shown in Figure 10. The feedforward and feedback integrated control is adopted for the direct yaw moment decision. Furthermore, the distribution of yaw moment between electric motors and the coordination control of electric motor driving system and hydraulic braking system are analyzed in detail.

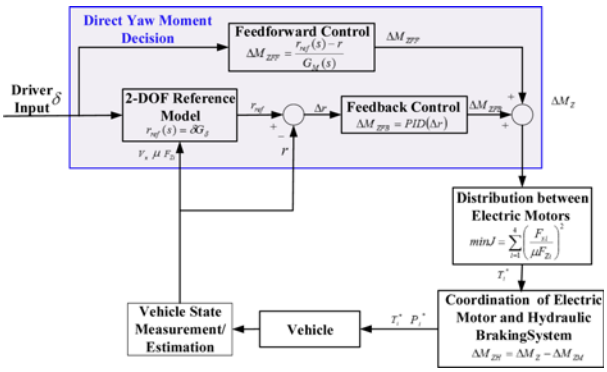

Figure 10. Structure diagram of direct yaw moment control system.

5.3.1. Yaw moment decision based on feedforward and feedback control

Based on the deviation of the current yaw rate and the reference yaw rate, the feedback control method has been widely used to calculate the desired yaw moment. Feedback control is a kind of closed-loop control which can keep the system with good steady-state performance. But the system dynamic performance is not always satisfactory. On the other hand, feedforward control calculate the control input based on the control object model. Then the input acts directly on the control object which is not necessary to go through the entire control loop. In this way, it can reach a faster response compared with feedback control method. However, due to model deviation and other disturbance, it is difficult for feedforward control to always give the exact control input. Therefore, a feedback control method combined with feedforward control is proposed to calculate the required additional yaw moment for stability control.

The 2 DOF reference vehicle model can be expressed as follows:

$$\begin{cases} mV_x(\dot{\beta} + r) = (K_f + K_r)\beta + \dfrac{L_a K_f - L_b K_r}{V_x} r - K_f \delta \\ I_Z \dot{r} = (L_a K_f - L_b K_r)\beta + \dfrac{L_a^2 K_f + L_b^2 K_r}{V_x} r - L_a K_f \delta \end{cases} \tag{12}$$

In the stability control system, the vehicle yaw rate can be considered to be generated by steering wheel input and differential driving/braking.

For the response characteristic of yaw rate to steering wheel angle in steady state, the $\dot{r}$ and $\dot{\beta}$ in Equation (12) are set to zero and the transfer function can be expressed as follows:

$$\frac{r}{\delta}(s) = G_\delta = \frac{u}{l(1 + KV_x^2)} \tag{13}$$

Then the reference yaw rate can be expressed as follows:

$$r_{\text{ref}}(s) = \delta G_\delta = \frac{u}{l(1 + KV_x^2)}\delta \tag{14}$$

For the response characteristic of yaw rate to yaw moment in steady state, the $\dot{\beta}$ and δ are set to zero and $I_Z \dot{r} = M_Z$, the transfer function can be expressed as follows:

$$\frac{r}{M_z}(s) = G_M = \frac{u(K_f + K_r)}{L^2 K_f K_r (1 + KV_x^2)} \tag{15}$$

Then the addition yaw moment required by feedforward

control can be expressed as follows:

$$\Delta M_{ZFF} = \frac{r_{ref}(s) - r}{G_M(s)} \tag{16}$$

Using a PI feedback control method, the additional yaw moment required by feedback control can be expressed as follows:

$$\Delta M_{ZFB} = K_P\left(r_{ref}(s) - r(s)\right) + K_I \int\left(r_{ref}(s) - r(s)\right)dt \tag{17}$$

After combination of the feedforward and feedback control, the total additional yaw moment requirement for stability control can be obtained:

$$\Delta M_Z = \Delta M_{ZFF} + \Delta M_{ZFB} \tag{18}$$

5.3.2. Yaw moment distribution among electric motors

As the electric motor torque can be controlled continuously and fast, the yaw moment will be firstly distributed between four electric motors. An optimal distribution method for minimum road adhesion consumption in longitudinal direction is used, of which the objective function can be expressed as follows:

$$min \quad J = \sum_{i=1}^{4}\left(\frac{F_{xi}}{\mu F_{Zi}}\right)^2 \tag{19}$$

where F_{xi} is the driving force of each wheel, F_{Zi} is the vertical load of each wheel.

The constraints can be expressed as follows:

$$s.t \begin{cases} \sum_{i=1}^{4} F_{xi} = f(\alpha_a) \\ (F_{x2} + F_{x4} - F_{x1} - F_{x3})\frac{D}{2} = \Delta M_Z \\ -min(\mu F_{Zi}, F_{max}) \le F_{xi} \le min(\mu F_{Zi}, F_{max}) \end{cases} \tag{20}$$

where α_a is acceleration pedal position, $f(\alpha_a)$ means the desired driving force determined by driver's operation, D is the thread, F_{max} is the maximum driving/braking force generated by the electric motor.

In above optimization problem, the optimization objective is the minimum overall longitudinal consumption of road adhesion. There is an inequality constraint about electric motor torque output limitation. Besides, there are two equality constraints. The first is to satisfy the driver's total driving torque requirement and the second is to satisfy the additional yaw moment requirement for stability control. The first equality constraint should be satisfied firstly, as it is the basic requirement for keep vehicle speed steady. On this premise, if the second constraint can't be satisfied, the hydraulic braking system will be started to supply the rest of yaw moment requirement.

5.3.3. Coordination control of electric motor and hydraulic braking system

The yaw moment generated by hydraulic braking system is the difference between the total additional yaw moment demand and the yaw moment supplied by electric motor, which can be expressed as follows:

$$\begin{cases} \Delta M_{ZM} = (F_{xd2} - F_{xd1} + F_{xd4} - F_{xd3}) \cdot \frac{d}{2} \\ \Delta M_{ZH} = \Delta M_Z - \Delta M_{ZM} \end{cases} \tag{21}$$

where ΔM_{ZM} is yaw moment that electric motor can supply, ΔM_{ZH} is the yaw moment required for hydraulic braking system, and $F_{xdi}(i = 1, 2, 3, 4)$ is the driving force of each electric motor. Because hydraulic braking usually works roughly with large intensity, just the best effect wheel is braked to generate the required yaw moment. The selection of the best effect wheel can refer to Wu *et al*. (2014).

According to the required yaw moment ΔM_{ZH}, the required additional braking pressure of the best effect wheel can be calculated:

$$\Delta P_{bi}^{*} = \frac{2 \cdot \Delta M_{ZH} R}{D \cdot K_{pbi}} \tag{22}$$

where K_{pbi} is the braking efficiency factor of a certain wheel.

6. SIMULATION AND ROAD TEST RESULTS

Simulation based on a FWID electric vehicle model is conducted. Then tests on a real vehicle with four in-wheel-motors are conducted for practical application of the proposed vehicle dynamics control system. Table 1 shows the nominal vehicle parameters.

6.1. Simulation Results

An open-loop maneuver on low adhesion road is simulated firstly, where the steering wheel input is a sine with dwell signal referring to the FMVSS126 standard (NHTSA, 2007). The tire-road friction coefficient is set as 0.2. The amplitude of steering wheel input is 30 deg and the initial vehicle speed is 80 km/h.

The simulation results can be seen in Figure 11. The performances of three control mode are compared: without

Table 1. Nominal vehicle parameters for simulation and road test.

Parameter	Value
Vehicle total mass m	1510 kg
Distance from C.G. to front axle L_a	1.3425 m
Distance from C.G. to rear axle L_b	1.3425 m
Yaw moment of inertia I_Z	3267 kg·m^2
Cornering stiffness of front tires K_f	60395 N/rad
Cornering stiffness of rear tires K_r	60655 N/rad
Electric motor maximum torque T_{max}	150 Nm
Electric motor power P_e	5 Kw

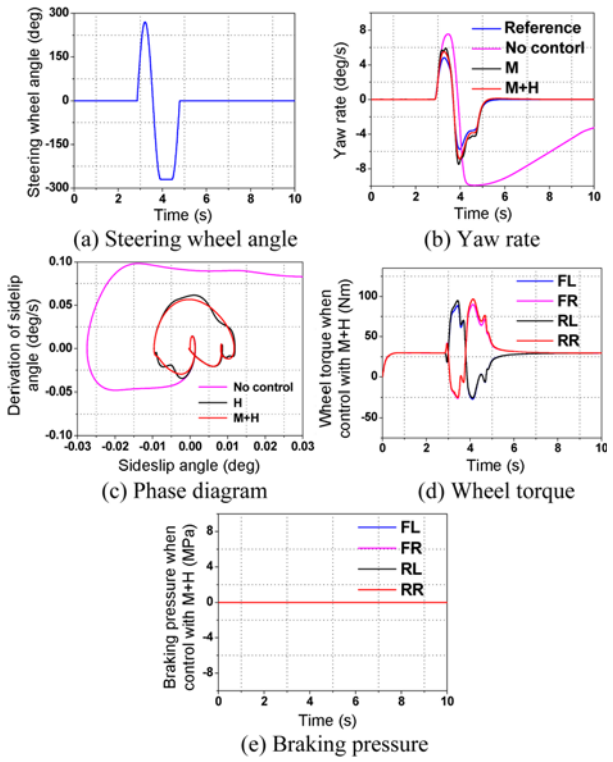

Figure 11. Simulation results of sine with dwell maneuver when tire-road friction coefficient is 0.2.

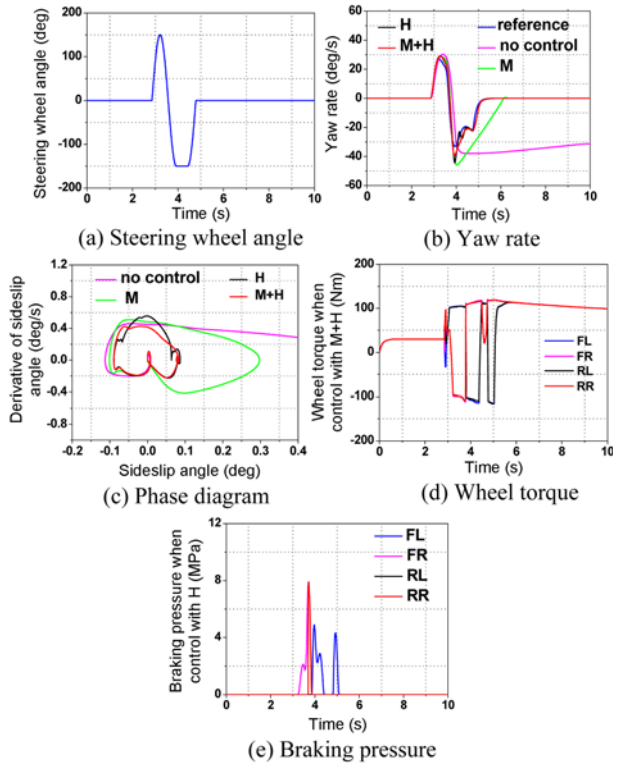

Figure 12. Simulation results of sine with dwell maneuver when tire-road friction coefficient is 0.8.

control represented by no control, the control actuated by conventional hydraulic braking system which represented by H, and the control actuated by both hydraulic braking system and electric motor which represented by M+H. From Figure 11 (c), it can be seen that the control by M+H can reach a smoother and faster state trajectory. This is mainly due to the faster response speed of electric motor torque. In Figure 11 (e), the braking pressure when control with M+H is always zero, *i.e.*, the hydraulic braking system is not started, which means that the electric motor can generate sufficient yaw moment. This indicates that the electric motor will play a key role when the yaw moment requirement is not too large on the low adhesion coefficient road. Besides, it can be seen from Figure 11 (d) that the driving torque is even distributed between four electric motors when the direct yaw moment control is not started. It is determined by the optimal torque distribution with maximum system efficiency in Section 2.

Then the amplitude of steering wheel input is increased to 150 deg. The tire-road friction coefficient is set as 0.8 and the initial vehicle speed is also 80 km/h. The simulation results can be seen in Figure 12. In order to evaluate the ability of electric motor, a control mode actuated only by electric motor is added for comparison, which is represented by M. In this condition, the maximum braking pressure when control by M+H is about 8 MPa, while control by M cannot reach the expected result. This indicates that the hydraulic braking system will play a key role when the yaw moment requirement is large. This is mainly due to the power limitation of electric motor.

(a) Road test ground (b) Sensors and actuators

Figure 13. Road test ground and the sensors and actuators of test FWID EV.

6.2. Road Test Results

The test electric vehicle with four in-wheel-motors is shown in Figure 13. A rapid prototype controller is used in the vehicle dynamics control system. The four in-wheel-motors and the electro-hydraulic braking system are controlled as actuators. Also some sensors are needed, such as the vehicle yaw rate and lateral acceleration sensor, wheel speed sensor and so on.

As the regenerative braking system is not developed in the vehicle, the electric motor is just used for differential driving during road test. And the differential braking is realized by EHB system. The sine with dwell open-loop

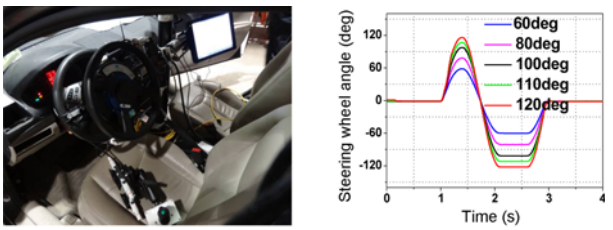

(a) Steering machine (b) Steering wheel input

Figure 14. Steering machine and steering wheel input of sine with dwell maneuver.

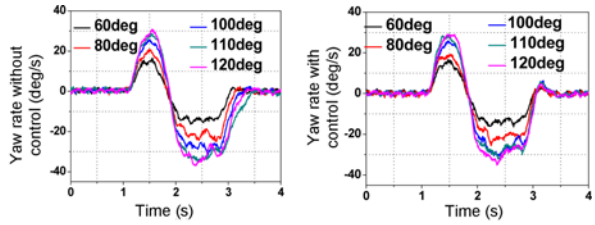

(a) Without control (b) With control

Figure 15. Comparison of the vehicle yaw rate in sine with dwell road test maneuver.

maneuver on a high adhesion road is conducted to verify the effect of the stability control with electric motor and EHB system as actuators.

The sine with dwell test is an open-loop maneuver which uses the steering machine for steering wheel input as shown in Figure 14.

The comparison of the vehicle yaw rate with increasing steering wheel angle is shown in Figure 15. The maximum amplitude of steering wheel input is 120 deg. In this condition, dynamics control system also contributes to improve the stability. During the time between 2.5 s and 3.5 s in Figure 15, the yaw rate without control returns to zero slowly and the return speed decreases as the steering wheel input amplitude increases. While the yaw rate with vehicle dynamics control can always return to zero rapidly in different steering wheel input amplitude. This is the time when vehicle most prone to lose stability, the rapid convergence of yaw rate is very important. The slow convergence will increase the risk of unstable.

The specific control process when the steering wheel input amplitude is 120 deg is shown in Figure 16. It can be seen that the electric motor torque is saturate in most of time. The hydraulic braking system is needed for compensatory.

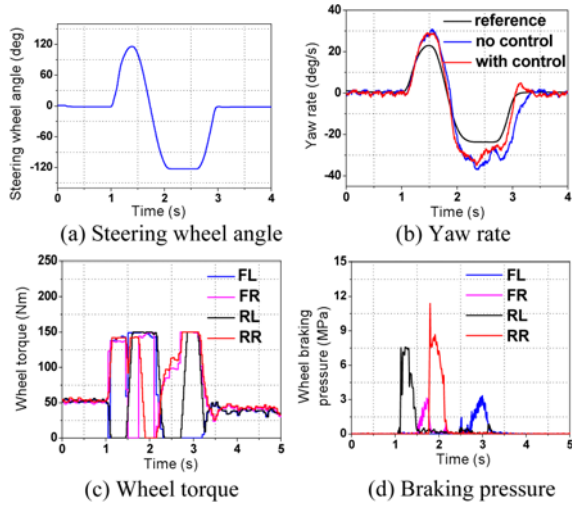

(a) Steering wheel angle (b) Yaw rate

(c) Wheel torque (d) Braking pressure

Figure 16. Control results of sine with dwell maneuver when the steering wheel input amplitude is 120 deg.

7. CONCLUSION

In this paper, the dynamics characteristics of FWID EV is evaluated through theoretical approach and validated in dynamics control. Several main conclusions are as follows:

(1) Firstly, even though the torque output amplitude is not as large as ICE and hydraulic braking system, the independent control of wheel driving torque can increase the vehicle available global lateral force and yaw moment significantly in the condition of low adhesion road, which can be used to improve the vehicle dynamics performance.

(2) Secondly, the increase in the controllable DOF provides possibility to improve the powertrain system efficiency through torque distribution between front and rear wheels. For the PMSM researched in this paper, the impact of idle loss on the torque distribution is significant. After considering the no-load loss, the optimal distribution ratio is always around 0.5 at any total torque demand.

(3) Besides, it indicates that the fast response of electric motor torque can increase the open-loop phase margin of direct yaw moment control system, which will be beneficial to improve the system relative stability.

(4) Taking full advantages of the controllable DOF and the fast torque respond speed, dynamics control of FWID EV based on the electric motor and hydraulic braking system improves the vehicle stability better than dynamics control based on the hydraulic braking system.

ACKNOWLEDGEMENT–This research is supported by National Natural Science Foundation of China (No. 51705383), the Foundation of State Key Laboratory of Automotive Simulation and Control (No. 20161103), and the Seed Foundation of Wuhan University of Technology (No. 2016IVA036).

REFERENCES

Chen, Y. and Wang, J. (2011). Fast and global optimal energy-efficient control allocation with applications to over-actuated electric ground vehicles. *IEEE Trans. Control Systems Technology* **20**, **5**, 1202–1211.

Chen, Y. and Wang, J. (2014). Design and experimental evaluations on energy efficient control allocation methods for overactuated electric vehicles: Longitudinal motion case. *IEEE/ASME Trans. Mechatronics* **19**, **2**, 538–548.

Dizqah, A. M., Lenzo, B., Sorniotti, A., Gruber, P., Fallah, S. and Smet, D. (2016). A fast and parametric torque distribution strategy for four-wheel-drive energy-efficient electric vehicles. *IEEE Trans. Industrial Electronics* **63**, **7**, 4367–4376.

Emırler, M. T., Kahraman, K., Şentürk, M., Acar, O. U., Güvenç Aksun, B., Güvenç, L. and Efendıoğlu, B. (2015). Lateral stability control of fully electric vehicles. *Int. J. Automotive Technology* **16**, **2**, 317–328.

Hac, A. and Simpson, M. (2000). Estimation of vehicle sideslip angle and yaw rate. *SAE Paper No*. 2000-01-0696.

Hori, Y. (2004). Future vehicle driven by electricity and control-research on four wheel motored "UOT Electric March II". *IEEE Trans. Industrial Electronics* **51**, **5**, 954–962.

Hu, J. S., Wang, Y., Fujimoto, H. and Hori, Y. (2017). Robust yaw stability control for in-wheel motor electric vehicles. *IEEE/ASME Trans. Mechatronics* **22**, **3**, 1360–1370.

Ivanov, V., Savitski, D., Augsburg, K., Barber, P., Knauder, B. and Zehetner, J. (2015). Wheel slip control for all-wheel drive electric vehicle with compensation of road disturbances. *J. Terramechanics*, **61**, 1–10.

Johansen, T. A. and Fossen, T. I. (2013). Control allocation – A survey. *Automatica* **49**, **5**, 1087–1103.

Jonasson, M., Andreasson, J., Jacobson, B. and Trigell, A. S. (2010). Global force potential of over-actuated vehicles. *Vehicle System Dynamics, Int. J. Vehicle Mechanics and Mobility* **48**, **9**, 983–998.

Jonasson, M., Andreasson, J., Solyom, S., Jacobson, B. and Trigell, A. S. (2011). Utilization of actuators to improve vehicle stability at the limit: From hydraulic brakes toward electric propulsion. *J. Dynamic Systems, Measurement, and Control* **133**, **5**, 502–506.

Sawase, K. and Ushiroda, Y. (2008). Improvement of vehicle dynamics by right-and-left torque vectoring system in various drivetrains. *Mitsubishi Technical Review* **2008**, **2**, 14–20.

Keiji, I. (1989). Effects on cornering characteristics by driven-force control. *J. Society of Automotive Engineers of Japan* **43**, **4**, 67–73.

Keiji, I. (1990). Technical trends of driving-force control technology. *J. Society of Automotive Engineers of Japan* **44**, **1**, 76–84.

Kim, H., Lee, S. and Hedrick, J. K. (2015). Active yaw control for handling performance improvement by using traction force. *Int. J. Automotive Technology* **16**, **3**, 457–464.

Kim, W., Yi, K. and Lee, J. (2012). An optimal traction, braking, and steering coordination strategy for stability and manoeuvrability of a six-wheel drive and six-wheel steer vehicle. *Proc. Institution of Mechanical Engineers, Part D: J. Automobile Engineering* **226**, **1**, 3–22.

Klomp, M. (2011). Longitudinal force distribution using quadratically constrained linear programming. *Vehicle System Dynamics, Int. J. Vehicle Mechanics and Mobility* **49**, **12**, 1823–1836.

Ko, S., Song, C. and Kim, H. (2016). Cooperative control of the motor and the electric booster brake to improve the stability of an in-wheel electric vehicle. *Int. J. Automotive Technology* **17**, **3**, 447–456.

Lin, C. and Xu, Z. (2015). Wheel torque distribution of four-wheel-drive electric vehicles based on multi-objective optimization. *Energies* **8**, **5**, 3815–3831.

Lu, D., Gu, J., Li, J., Ouyang, M. and Ma, Y. (2009). High-performance control of PMSM based on a new forecast algorithm with only low-resolution position sensor. *Vehicle Power and Propulsion Conf., IEEE*, 1440–1444.

Lv, C., Zhang, J., Li, Y., Sun, D. and Yuan, Y. (2014). Hardware-in-the-loop simulation of pressure-difference-limiting modulation of the hydraulic brake for regenerative braking control of electric vehicles. *Proc. Institution of Mechanical Engineers, Part D: J. Automobile Engineering* **228**, **6**, 649–662.

Lv, C., Zhang, J., Li, Y. and Yuan, Y. (2015). Mechanism analysis and evaluation methodology of regenerative braking contribution to energy efficiency improvement of electrified vehicles. *Energy Conversion and Management*, **92**, 469–482.

Lv, C., Wang, H. and Cao, D. (2017). High-precision hydraulic pressure control based on linear pressure-drop modulation in valve critical equilibrium state. *IEEE Trans. Industrial Electronics*, **99**, 1.

NHTSA (2007). Electronic Stability Control Systems. Federal Motor Vehicle Safety Standard 126.

Novellis, L. D., Sorniotti, A. and Gruber, P. (2014). Wheel torque distribution criteria for electric vehicles with torque-vectoring differentials. *IEEE Trans. Vehicular Technology* **63**, **4**, 1593–1602.

Ogata, K. (2009). *Modern Control Engineering*. 5th edn. Pearson Custom Publishing. Boston, USA.

Park, J., Jeong, H., Jang, I. and Hwang, S. H. (2015). Torque distribution algorithm for an independently driven electric vehicle using a fuzzy control method. *Energies* **8**, **8**, 8537–8561.

Phanomchoeng, G., Rajamani, R. and Piyabongkarn, D. (2011). Nonlinear observer for bounded jacobian systems, with applications to automotive slip angle estimation. *IEEE Trans. Automatic Control* **56**, **5**, 1163–1170.

Piyabongkarn, D., Rajamani, R., Grogg, J. A. and Lew, J. Y. (2009). Development and experimental evaluation of a slip angle estimator for vehicle stability control. *IEEE Trans. Control Systems Technology* **17**, **1**, 78–88.

Shuai, Z., Zhang, H., Wang, J., Li, J. and Ouyang, M. (2014). Lateral motion control for four-wheel-independent-drive electric vehicles using optimal torque allocation and

dynamic message priority scheduling. *Control Engineering Practice*, **24**, 55–66.

Wang, Y., Nguyen, B. M., Fujimoto, H. and Hori, Y. (2014). Multirate estimation and control of body slip angle for electric vehicles based on onboard vision system. *IEEE Trans. Industrial Electronics* **61**, **2**, 1133–1143.

Wu, D., Ding, H., Guo, K. and Wang, Z. (2014). Experimental research on the pressure following control of electro-hydraulic braking system. *SAE Paper No*. 2014-01-0848.

Xiong, L., Teng, G. W., Yu, Z. P., Zhang, W. X. and Feng, Y. (2016). Novel stability control strategy for distributed drive electric vehicle based on driver operation intention. *Int. J. Automotive Technology* **17**, **4**, 651–663.

Yim, S. (2017). Coordinated control of ESC and AFS with adaptive algorithms. *Int. J. Automotive Technology* **18**, **2**, 271–277.

Yin, D. and Hu, J. S. (2014). Active approach to electronic stability control for front-wheel drive in-wheel motor electric vehicles. *Int. J. Automotive Technology* **15**, **6**, 979–987.

Yin, G., Wang, R. and Wang, J. (2015). Robust control for four wheel independently-actuated electric ground vehicles by external yaw-moment generation. *Int. J. Automotive Technology* **16**, **5**, 839–847.

Yoon, J. H. and Peng, H. (2014). A cost-effective sideslip estimation method using velocity measurements from two GPS receivers. *IEEE Trans. Vehicular Technology* **63**, **6**, 2589–2599.

Yu, N. and Gong, Y. M. (2008). High dynamic performance speed control strategy of high density IPMSM for HEV application. *Intelligent Control and Automation, 7th World Cong*., 1588–1593.

Yu, Z., Yang, P. and Xiong, L. (2014). Application of control allocation in distributed drive electric vehicle. *J. Mechanical Engineering*, **18**, 99–107.

Zhao, H., Ren, B., Chen, H. and Deng, W. (2015). Model predictive control allocation for stability improvement of four-wheel drive electric vehicles in critical driving condition. *IET Control Theory & Applications* **9**, **18**, 2688–2696.